CSMA 2024
16ème Colloque National en Calcul des Structures
13-17 Mai 2024, Presqu'île de Giens (Var)

Exact energy-conserving and linear discretization scheme for geometrically non-linear models

A. Brugnoli[1], D. Matignon[2], J. Morlier[1]

[1] *ICA, Université de Toulouse, ISAE-SUPAERO, MINES ALBI, UPS, INSA, CNRS, Toulouse, France*
[2] *ISAE-SUPAERO, Université de Toulouse, France*

Résumé — In this contribution, we discuss a discretization scheme for geometrically non linear mechanical models that give rise to an exact energy balance, but only requires a solution of a linear system. The system is rewritten in Hamiltonian form using a Poisson bracket. By combining an implicit midpoint integration on the energy part and a Störmer-Verlet integrator for the displacement-like variable, the resulting scheme conserves the energy exactly, while only requiring the solution of a linear system
Mots clés — Hamiltonian dynamics, finite elements, energy conservation, symplectic integration

1 Introduction

When solving dynamical problems in structural mechanics, several time integration scheme can be used. These methods may provide exact energy preservation or approximate energy preservation [2]. Approximate energy conservation is obtained by exactly preserving a pseudo-energy. This is a typical feature of symplectic methods, whose the most prominent representative is the Störmer-Verlet method. Recently, Bilbao and co-authors have discussed an explicit method capable of exactly preserving the energy of Hamiltonian systems [1]. This method can be applied to problems with positive definite potential energy, since then a new variable, corresponding to the square root of the potential energy, is well defined. A in-depth mathematical analysis of a quadratization strategy for geometrically non-linear strings in given in [10].

In this contribution we show how some geometrically non-linear problems in mechanics can be simulated via a linearly implicit scheme that preserves the energy exactly. This result is achieved thanks to the choice of unknown variables and depends on the choice of constitutive law used for the model. In the Saint-Venant Kirchhoff law, the deformation energy is quadratic in the the second Piola stress tensor. Introducing this variable as an additional unknown leads to a mixed formulation where the non linearity is only due to the deformation gradient. The energy can then be exactly preserved using an implicit midpoint method on the part of the system featuring the velocity field and second Piola stress tensor (which are the variables related to the energy). A linear scheme is then obtained by staggering in time the integration of the deformation gradient using a Störmer-Verlet integration [11].

2 Example of non-linear model in mechanics

In this section, we briefly recall the general non-linear elastodynamics problem and the von Kármán plate problem. These models share a very similar structure that can be exploited by numerical methods. In the following the Hamiltonian structure of these models will be highlighted.

2.1 Non-linear elastodynamics

The material description of non-linear elasticity in a bounded domain $\Omega \in \mathbb{R}^d$, $d = \{2,3\}$ with boundary $\partial\Omega = \Gamma_1 \cup \Gamma_2$ is given by the following equation

$$\begin{aligned} \partial_t \boldsymbol{u} &= \boldsymbol{v}, & \boldsymbol{u}(\boldsymbol{x},0) &= \boldsymbol{u}_0(\boldsymbol{x}), & \boldsymbol{u}(\boldsymbol{x},0)|_{\Gamma_1} &= \boldsymbol{0}, \\ \rho\partial_t \boldsymbol{v} &= \mathrm{div}(\boldsymbol{F}\boldsymbol{S}), & \boldsymbol{v}(\boldsymbol{x},0) &= \boldsymbol{v}_0(\boldsymbol{x}), & \boldsymbol{F}\boldsymbol{S}\boldsymbol{n}|_{\Gamma_2} &= \boldsymbol{t}, \end{aligned}$$

where ρ is the density, $\boldsymbol{u}(\boldsymbol{x},t) : \Omega \times \mathbb{R}_+ \to \mathbb{R}^d$ is the displacement field and $\boldsymbol{S}(\boldsymbol{x},t) : \Omega \times \mathbb{R}_+ \to \mathbb{R}^{d\times d}_{\text{sym}}$ is the second Piola stress tensor, $\boldsymbol{F} = \boldsymbol{I} + \nabla \boldsymbol{u} : \Omega \times \mathbb{R}_+ \to \mathbb{R}^{d\times d}$ is the deformation gradient, and $\boldsymbol{n}$ is the outward unit normal. We now make the assumption that the material follows a Saint-Venant Kirchhoff law, meaning that

$$\boldsymbol{S} = \mathcal{K}\boldsymbol{E}, \qquad \boldsymbol{E} := \boldsymbol{F}^\top \boldsymbol{F} - \boldsymbol{I},$$

where $\mathcal{K}(\circ) = \frac{E\nu}{(1+\nu)(1-2\nu)} \boldsymbol{I}\,\mathrm{tr}(\circ) + \frac{E}{1+\nu}(\circ) \in \mathbb{R}^{d\times d}_{\text{sym}} \to \mathbb{R}^{d\times d}_{\text{sym}}$ is the stiffness tensor, and $\boldsymbol{E}$ is the Green-Lagrange strain tensor. By introducing the dynamical equation for the second Piola stress tensor, the Hamiltonian structure of the equations can be highlighted [4] :

$$\begin{aligned} \partial_t \boldsymbol{F} &= \nabla \boldsymbol{v}, \\ \begin{bmatrix} \rho & 0 \\ 0 & \mathcal{C} \end{bmatrix} \frac{\partial}{\partial t} \begin{pmatrix} \boldsymbol{v} \\ \boldsymbol{S} \end{pmatrix} &= \underbrace{\begin{bmatrix} 0 & \mathrm{div}(\boldsymbol{F}\circ) \\ \mathrm{sym}(\boldsymbol{F}^\top \nabla \circ) & 0 \end{bmatrix}}_{\mathcal{J}_E} \begin{pmatrix} \boldsymbol{v} \\ \boldsymbol{S} \end{pmatrix}, \end{aligned}$$

The $\circ$ indicates where the variables $\boldsymbol{v}$, $\boldsymbol{S}$ appear in the $\mathcal{J}_E$ operator. $\mathcal{C} := \mathcal{K}^{-1}$ is the compliance tensor, $\mathrm{sym}(\boldsymbol{A}) := \frac{1}{2}(\boldsymbol{A} + \boldsymbol{A}^\top) : \mathbb{R}^{d\times d} \to \mathbb{R}^{d\times d}$ is the symmetrization operator. The operator $\mathcal{J}_E$ is formally skew-adjoint in the sense that

$$(\boldsymbol{\alpha}, \mathcal{J}_E \boldsymbol{\beta})_\Omega = -(\mathcal{J}_E \boldsymbol{\alpha}, \boldsymbol{\beta})_\Omega, \qquad \boldsymbol{\alpha}, \boldsymbol{\beta} \in \mathbb{R}^d \times \mathbb{R}^{d\times d}_{\text{sym}} \tag{1}$$

where $(\cdot,\cdot)_\Omega$ is the inner product over $L^2(\Omega;\mathbb{R}^d) \times L^2(\Omega;\mathbb{R}^{d\times d}_{\text{sym}})$ and $\boldsymbol{\alpha}, \boldsymbol{\beta}$ vanish at the boundary.

In this formulation, the energy is given by

$$H = \frac{1}{2} \int_\Omega \rho ||\boldsymbol{v}||^2 + \boldsymbol{S} : \mathcal{K}\boldsymbol{S}\, \mathrm{d}\Omega$$

It can be noticed that this selection of variables is such that it makes the energy quadratic. This is important as it is therefore possible to exploit the quadratisation of the energy to design a linearly implicit scheme [1].

Using the skew-adjoint property (1), the energy rate is computed+ :

$$\dot{H} = \int_{\Gamma_2} \boldsymbol{v} \cdot \boldsymbol{t}\, \mathrm{d}s. \tag{2}$$

This means that the energy can only change due to a power flow through the Γ_2 part of the boundary $\partial\Omega$.

2.2 Von-Kármán plate

One of the classical dynamical models for geometrically non-linear plates is the model is the von-Kármán one, defined in a planar two dimensional domain $\Omega \in \mathbb{R}^2$ [5]

$$\begin{aligned} \partial_t \boldsymbol{u}_m &= \boldsymbol{v}_m, \\ \partial_t u_z &= v_z, \\ \rho h \partial_t \boldsymbol{u}_m &= \mathrm{div}(\boldsymbol{N}), \\ \rho h \partial_t u_z &= -\,\mathrm{div}\,\mathrm{div}\,\boldsymbol{M} + \mathrm{div}(\boldsymbol{N}\nabla u_z), \end{aligned}$$

where h is the plate thickness, $\boldsymbol{u}_m : \Omega \times \mathbb{R}_+ \to \mathbb{R}^2$ is the in-plane displacement, $u_z : \Omega \times \mathbb{R}_+ \to \mathbb{R}$ is the vertical displacement, $\boldsymbol{N} : \Omega \times \mathbb{R}_+ \to \mathbb{R}^{2\times 2}_{\text{sym}}$ is the in-plane stress tensor, and $\boldsymbol{M} : \Omega \times \mathbb{R}_+ \to \mathbb{R}^{2\times 2}_{\text{sym}}$ is the bending stress tensor. The model is completed once initial data have been defined and boundary conditions have been prescribed. The derivation of the boundary conditions for this model is more involved as a second order differential operator has to be considered. Therefore, we omit it, since this is not crucial for the present discussion. Again a linear elastic constitutive relation is assumed

$$\boldsymbol{N} = \mathcal{K}_m\, \mathrm{sym}(\nabla \boldsymbol{u}_m), \qquad \boldsymbol{M} = \mathcal{K}_b\, \mathrm{hess}\, u_z,$$

where $\mathcal{K}_m$, $\mathcal{K}_b$ are the membrane and bending system. By introducing the dynamics of the membrane and bending stresses, the Hamiltonian structure of the problem becomes apparent

$$\partial_t \boldsymbol{f}_z = \nabla v_z,$$
$$\begin{bmatrix} \rho h & 0 & 0 & 0 \\ 0 & \rho h & 0 & 0 \\ 0 & 0 & \mathcal{K}_m^{-1} & 0 \\ 0 & 0 & 0 & \mathcal{K}_b^{-1} \end{bmatrix} \frac{\partial}{\partial t} \begin{pmatrix} \boldsymbol{v}_m \\ v_z \\ \boldsymbol{N} \\ \boldsymbol{M} \end{pmatrix} = \underbrace{\begin{bmatrix} 0 & 0 & \operatorname{div} & 0 \\ 0 & 0 & \operatorname{div}(\circ \boldsymbol{f}_z) & -\operatorname{div}\operatorname{div} \\ \operatorname{sym}\nabla & \operatorname{sym}(\nabla \circ \otimes \boldsymbol{f}_z) & 0 & 0 \\ 0 & \operatorname{hess} & 0 & 0 \end{bmatrix}}_{\mathcal{J}_{VK}} \begin{pmatrix} \boldsymbol{v}_m \\ v_z \\ \boldsymbol{N} \\ \boldsymbol{M} \end{pmatrix},$$

Again, the $\circ$ indicates where the variables appear in the different operators. The symbol $\otimes$ denotes the dyadic product. The same properties previously discussed for the non-linear elastodynamic model carry over to this example. In particular, the operator $\mathcal{J}_{VK}$ is formally skew-adjoint. The structure of these two examples, given by a skew-symmetric operator modulated by a deformation gradient, is essentially the same. A very similar system is obtained in the case in which shear deformability is also taken into account.

3 Exact energy conservation via an implicit linear scheme

The numerical scheme will be discussed for the non-linear elastodynamics only for sake of simplicity. Similar arguments can be used for the von Kàrmàn model. However this latter case is complicated by the presence of higher order differential operators. The use of distributional finite elements (e.g. the Hellan-Hermann Johnson element) may be more appealing in this case than the conforming ones (like the Argyris or Bell elements). Indeed conforming elements are very high dimensional (27 dofs per triangle for the Argyris element) and lead to ill-conditioned mass matrices.

3.1 Spatial discretization

A mixed finite element formulation will be used to obtain the discrete model. Given a simplicial mesh $\mathcal{T}_h$, we introduce discrete space for the variables

$$M_h = \{\boldsymbol{F}_h|_T \in [\mathbb{P}_{k-1}]^{d\times d},\ \forall T \in \mathcal{T}_h\}, \quad \text{Discontinuous matrix-valued space of order } k-1,$$
$$V_h = \{\boldsymbol{v}_h \in C^0(\Omega), \quad \boldsymbol{v}_h|_T \in [\mathbb{P}_k]^d,\ \forall T \in \mathcal{T}_h\}, \quad \text{Lagrange finite element of order } k$$
$$\Sigma_h = \{\boldsymbol{S}_h|_T \in [\mathbb{P}_{k-1}]^{d\times d}_{\operatorname{sym}},\ \forall T \in \mathcal{T}_h\}, \quad \text{Discontinuous symmetric matrix-valued space of order } k-1.$$

The following weak formulation is then used for the discretization : find $\boldsymbol{F}_h \in M_h$, $\boldsymbol{v}_h \in V_h$, $\boldsymbol{S}_h \in \Sigma_h$ such that it holds

$$\begin{aligned} (\boldsymbol{\Psi}_F, \partial_t \boldsymbol{F}_h)_\Omega &= (\boldsymbol{\Psi}_F, \nabla \boldsymbol{v}_h)_\Omega, && \forall \boldsymbol{\Psi}_F \in M_h, \\ (\boldsymbol{\psi}_v, \rho \partial_t \boldsymbol{v}_h)_\Omega &= -(\nabla \boldsymbol{\psi}_v, \boldsymbol{F}_h \boldsymbol{S}_h)_\Omega + (\boldsymbol{\psi}_v, \boldsymbol{t})_{\Gamma_2}, && \forall \boldsymbol{\psi}_v \in V_h(\Gamma_1), \\ (\boldsymbol{\Psi}_S, \mathcal{C} \partial_t \boldsymbol{S}_h)_\Omega &= (\boldsymbol{\Psi}_S, \operatorname{sym} \boldsymbol{F}^\top \nabla \boldsymbol{v}_h)_\Omega, && \forall \boldsymbol{\Psi}_S \in \Sigma_h. \end{aligned}$$

where $V_h(\Gamma_1)$ is the subspace of V_h that vanishes on Γ_1. Given a finite element basis, with spanning elements $\boldsymbol{\Xi}_F, \boldsymbol{\xi}_v, \boldsymbol{\Xi}_S$, the following algebraic realization of the system is obtained :

$$\mathbf{M}\dot{\mathbf{f}} = \mathbf{D}\,\mathbf{v},$$
$$\begin{bmatrix} \mathbf{M}_\rho & 0 \\ 0 & \mathbf{M}_C \end{bmatrix} \begin{pmatrix} \dot{\mathbf{v}} \\ \dot{\mathbf{s}} \end{pmatrix} = \underbrace{\begin{bmatrix} 0 & -\mathbf{G}(\mathbf{f})^\top \\ \mathbf{G}(\mathbf{f}) & 0 \end{bmatrix}}_{\mathbf{J}_E} \begin{pmatrix} \mathbf{v} \\ \mathbf{s} \end{pmatrix} + \begin{pmatrix} \mathbf{t} \\ \mathbf{0} \end{pmatrix}, \tag{3}$$

The matrices are defined as follows

$$\mathbf{M}^{ij} = (\boldsymbol{\Xi}_F^i, \boldsymbol{\Xi}_F^j)_\Omega, \qquad \mathbf{M}_\rho^{ij} = (\boldsymbol{\xi}_v^i, \rho \boldsymbol{\xi}_v^j)_\Omega, \qquad \mathbf{M}_C^{ij} = (\boldsymbol{\Xi}_S^i, \mathcal{C}\boldsymbol{\Xi}_S^j)_\Omega,$$
$$\mathbf{D}^{ij} = (\boldsymbol{\Xi}_F^i, \nabla \boldsymbol{\xi}_v^j)_\Omega, \qquad \mathbf{G}^{ijk} = (\boldsymbol{\Xi}_S^i, \operatorname{sym} \boldsymbol{\Xi}_F^{\top,k} \nabla \boldsymbol{\xi}^j)_\Omega.$$

where $\mathbf{G}^{ijk}$ is a third-order tensor. This mixed discretization immediately leads to a discrete version of the power balance : this is a direct consequence of the fact that the matrix $\mathbf{J}_E$ is skew symmetric. Indeed the discrete energy reads

$$H_d = \frac{1}{2}(\mathbf{v}^\top \mathbf{M}_\rho \mathbf{v} + \mathbf{s}^\top \mathbf{M}_C \mathbf{s}).$$

The energy rate is then given by

$$\dot{H}_d = \mathbf{v}^\top \mathbf{t}. \tag{4}$$

3.2 Time integration

The time-integration schemes exploits the fact that the non-linearity in system (3) only comes from the deformation gradient. To achieve exact energy conservation, the dynamics due to the velocity and the second Piola stress tensor has to be integrated using an implicit midpoint method. The dynamical equation for the deformation gradient is instead integrated on a staggered grid, as in a Störmer-Verlet scheme. To this aim, let us consider a constant time step Δt and equispaced simulation instants $t_n = n\Delta t$.

$$\mathbf{M}(\mathbf{f}_{n+1/2} - \mathbf{f}_{n-1/2}) = \Delta t\, \mathbf{D}\, \mathbf{v}_n, \tag{5}$$

$$\begin{bmatrix} \mathbf{M}_\rho & 0 \\ 0 & \mathbf{M}_C \end{bmatrix} \begin{pmatrix} \mathbf{v}_{n+1} - \mathbf{v}_n \\ \mathbf{s}_{n+1} - \mathbf{s}_n \end{pmatrix} = \frac{\Delta t}{2} \begin{bmatrix} 0 & -\mathbf{G}(\mathbf{f}_{n+1/2})^\top \\ \mathbf{G}(\mathbf{f}_{n+1/2}) & 0 \end{bmatrix} \begin{pmatrix} \mathbf{v}_{n+1} + \mathbf{v}_n \\ \mathbf{s}_{n+1} + \mathbf{s}_n \end{pmatrix} + \Delta t \begin{pmatrix} \mathbf{t}_{n+1/2} \\ \mathbf{0} \end{pmatrix}, \tag{6}$$

To start the algorithm, the value $\mathbf{f}_{1/2}$ needs to be known. It can be obtained using an explicit Euler method :

$$\mathbf{M}\mathbf{f}_{1/2} = \mathbf{M}\mathbf{f}_0 + \frac{\Delta t}{2}\mathbf{D}\,\mathbf{v}_0.$$

This scheme only requires the solution of a linear system. The first one is given by a positive symmetric matrix, the second one by the sum of a positive symmetric matrix and a skew-symmetric one. Multiplting Eq. (6) by the vector $(\mathbf{v}_{n+1/2}^\top \quad \mathbf{s}_{n+1/2}^\top)^\top$, the following discrete energy balance is obtained

$$H_{d,n+1} - H_{d,n} = \Delta t\, \mathbf{v}_{n+1/2}^\top \mathbf{t}_{n+1/2}.$$

This balance thus mimicks its time continuous counterpart (5). The displacement can be reconstructed a posteriori, using the trapezoidal rule

$$\mathbf{u}_{n+1} = \mathbf{u}_n + \Delta t\, \mathbf{v}_{n+1/2}.$$

The scheme is therefore second-order accurate in time.

4 Numerical example

As a numerical example, we study a cantilever beam subject to a transverse load. The physical parameters are chosen to $\rho = 1[\mathrm{kg/m^3}]$, $E = 1000[\mathrm{Pa}]$, $\nu = 0.3$. The total simulation time is set to $T_{\mathrm{end}} = 10[\mathrm{s}]$ and the time step to $\Delta t = 0.01[\mathrm{s}]$. The polynomial degree is taken to be $k = 1$ and 100 elements are chosen along the x axis and 10 elements are chosen along the y axis. The boundary condition is a vertical follower force having expression

$$\boldsymbol{t} = \boldsymbol{F} \begin{bmatrix} 0, \\ 50\, t/t_{\mathrm{cutoff}} \end{bmatrix} [\mathrm{Pa}],$$

where $t_{\mathrm{cutoff}} = 5[\mathrm{s}]$. The experiment is carried out using FIREDRAKE [9]. Snapshots of the displacement field are reported in Fig. 2, where the linear and non-linear simulations are compared. The non-linear simulation clearly shows a more realistic behaviour, where the beam shortens along the x axis. The energy trend is shown in Fig. 1a. As one would expect, the energy increase due to the forcing is lower in the non-linear case. Both simulations do preserve the energy balance up to machine precision (see Fig. 1b). In the non-linear simulation however, the displacement field leads some mesh elements to overlap (cf. Fig. 2h at $x = 55, y = 15$). This leads to an unphysical solution for which the deformation gradient has determinant equal to zero, or even negative. This problem may be alleviated using an adaptive mesh strategy in regions subject to high distorsion. This problem may be due to the given formulation and to the choice of the finite element basis. Alternative formulations might be used to avoid this issue.

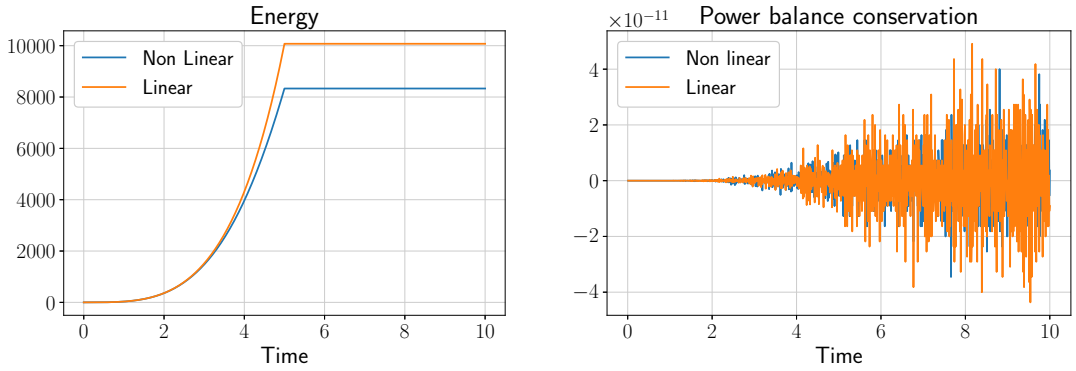

(a) Energy

(b) Power balance

FIGURE 1 – Energy trend and conservation of the power balance. The energy stored in the non-linear case is less than in the linear case. The power balance reported in Eq. 2 is drawn on the right.

5 Conclusion

In this contribution, we discussed the implementation of an implicit linear scheme for Saint-Venant Kirchhoff materials. The same strategy can also be employed to simulate the behaviour of thin models of von Kármán type. The time integration exploits the special structure of the problem and handles the non-linearity via a Störmer-Verlet scheme. Extensions to neo-Hookean materials will be the object of subsequent investigations.

Références

[1] Bilbao, S., Ducceschi, M., and Zama, Z. *Explicit exactly energy-conserving methods for Hamiltonian systems.* Journal of Computational Physics, 472 (2023) : 111697.

[2] Hughes, T. J. R., Caughey, T. K., and Liu, W. K. (June 1, 1978). *Finite-Element Methods for Nonlinear Elastodynamics Which Conserve Energy.* ASME. J. Appl. Mech., 45.2 (1978) : : 366–370.

[3] Simo, Juan C., Tarnow, N. and Wong, K. *Exact energy-momentum conserving algorithms and symplectic schemes for nonlinear dynamics.* Computer Methods in Applied Mechanics and Engineering 100.1 (1992) : 63-116.

[4] Thoma, T., Kotyczka, P. *Explicit port-Hamiltonian FEM models for geometrically nonlinear mechanical systems.* Arxiv preprint 2202.02097, submitted to Mathematical and Computer Modelling of Dynamical Systems (MCMDS)

[5] Bilbao, S., Thomas, O., Touzé, C., and Ducceschi, M. *Conservative numerical methods for the full von Kármán plate equations.* Numerical Methods for Partial Differential Equations, 31.6 (2015) : 1948–1970.

[6] Sato, S., Yuto M., and John C. B.. *High-order linearly implicit schemes conserving quadratic invariants.* Applied Numerical Mathematics 187 (2023) : 71-88.

[7] Brugnoli, A., Rashad, R., Califano, F., Stramigioli, S. and Matignon, D. *Mixed finite elements for port-Hamiltonian models of von Kármán beams*. IFAC-PapersOnLine 54(19), 186–191, 2021. In Proc. 7th IFAC Workshop on Lagrangian and Hamiltonian Methods for Nonlinear Control LHMNC 2021.

[8] Kinon, P. L., Thoma, T., Betsch, P., and Kotyczka, P. *Discrete nonlinear elastodynamics in a port-Hamiltonian framework*. Proceedings in Applied Mathematics and Mechanics (2023).

[9] Rathgeber, F., Ham, D.A., Mitchell, L., Lange, M., Luporini, F., Mcrae A.T.T., Bercea, G.T., Markall, G.R., and Kelly, P.H.J. *Firedrake : Automating the Finite Element Method by Composing Abstractions*. ACM Trans. Math. Softw. 43, 3, Article 24 (2017), 27 pages. https ://doi.org/10.1145/2998441

[10] Castera, G. and Chabassier, J. *Numerical analysis of quadratized schemes. Application to the simulation of the nonlinear piano string*. Research Report n° 9516, Inria (2023), 53 pages.

[11] Hairer, E., Lubich, C. and Wanner, G. *Geometric numerical integration illustrated by the Störmer–Verlet method*. Acta Numerica. Cambridge University Press, 12 (2003), pp. 399–450.

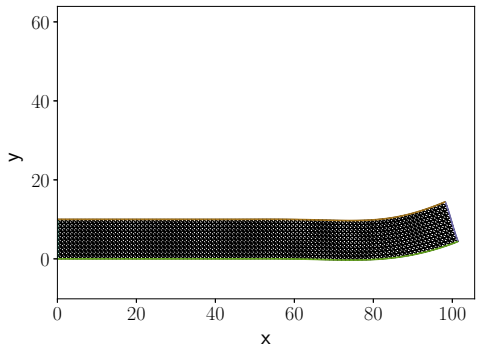

(a) Linear $t = 2.5$ [s]

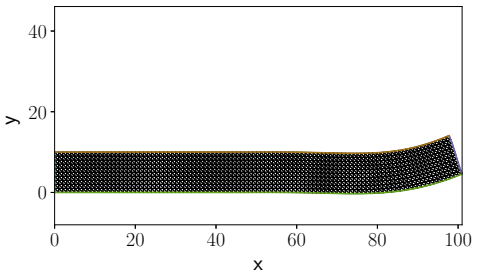

(b) Non linear $t = 2.5$ [s]

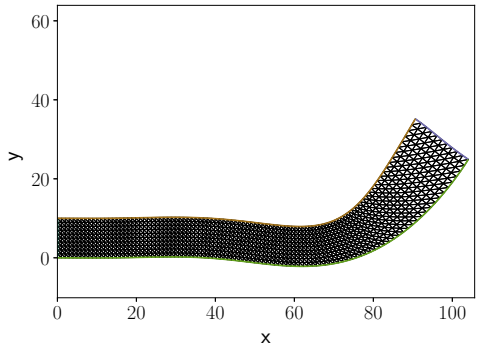

(c) Linear $t = 5$ [s]

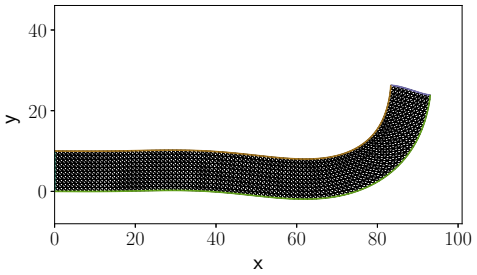

(d) Non linear $t = 5$ [s]

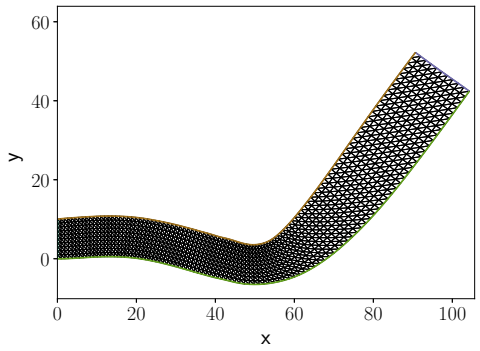

(e) Linear $t = 7.5$ [s]

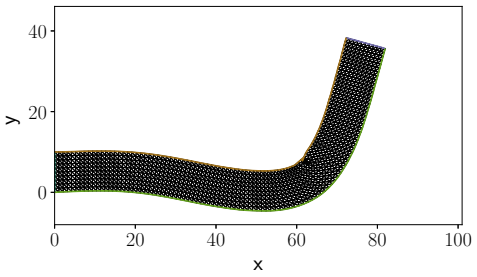

(f) Non linear $t = 7.5$ [s]

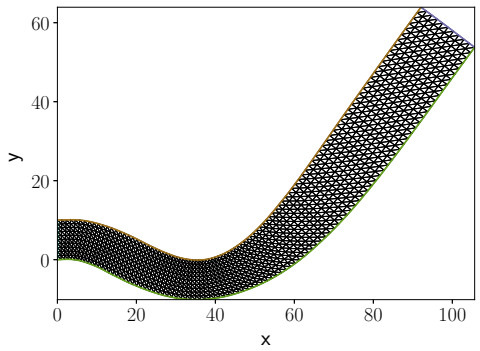

(g) Linear $t = 10$ [s]

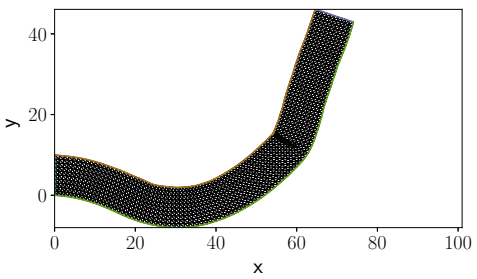

(h) Non linear $t = 10$ [s]

FIGURE 2 – Displacement field for the linear and non-linear problem.